Elsevier Editorial System(tm) for Ceramics International

Manuscript Draft

Manuscript Number: CERI-D-16-07308

Title: Structural and mechanical properties of La0.6Sr0.4M0.1Fe0.9O3-δ (M: Co, Ni and Cu) perovskites

Article Type: Full length article

Keywords: Perovskite; ultrasound assisted synthesis; structure; mechanical properties.

Corresponding Author: Dr. Ali Akbari-Fakhrabadi, Ph.D.

Corresponding Author's Institution: University of Chile

First Author: Ali Akbari-Fakhrabadi, Ph.D.

Order of Authors: Ali Akbari-Fakhrabadi, Ph.D.; V. Meruane, PhD; M. Jamshidijam, PhD; M.A. Gracia-Pinilla; R. Garcia, PhD; M. Orellana

Abstract: La0.6Sr0.4M0.1Fe0.9O3-δ (M: Co, Ni and Cu) perovskite nanostructures were synthesized using low frequency ultrasound assisted synthesis technique and effect of substitution of Fe by Co, Ni and Cu on crystal structure and mechanical properties in La0.6Sr0.4FeO3-δ perovskite were studied. The HRTEM and Rietveld refinement analyses revealed the uniform equi-axial shape of the obtained nanostructures with the existence of La0.6Sr0.4M0.1Fe0.9O3−δ with mixed rhombohedral and orthorhombic structures. Substitution of Cu decreases the melting point of La0.6Sr0.4FeO3-δ. The results of mechanical characterizations show that La0.6Sr0.4Co0.1Fe0.9O3−δ and La0.6Sr0.4Ni0.1Fe0.9O3−δ have ferroelastic behavior and comparable elastic moduli, however, subtitution of Ni shows higher hardness and lower fracture toughness than Co in B-site doping.

Suggested Reviewers: Siew Hwa Chan professor
Mechanical Engineering, Nanyang Technological University
MSHCHAN@ntu.edu.sg

San Ping Jiang
University of Curtin
S.Jiang@curtin.edu.au

Rose-Noelle Vannier
Ecole Nationale Supérieure de Chimie de Lille, France
rose-noelle.vannier@ensc-lille.fr

Opposed Reviewers:

Cover Letter

FACULTAD DE CIENCIAS FÍSICAS Y MATEMÁTICAS
UNIVERSIDAD DE CHILE

To

Date: 03.10.2016

Professor P. Vincenzini
The General Editor
Ceramics International

Dear Professor/Editor,

Sub: Submission of manuscript - reg.

Greetings. I herewith am submitting one of our research manuscripts entitled**, "Structural and mechanical properties of $La_{0.6}Sr_{0.4}M_{0.1}Fe_{0.9}O_{3-\delta}$ (M: Co, Ni and Cu) perovskites"** for favor publishing in your esteemed Journal, **Ceramics International**.

This manuscript reports the characteristics such as structure, phase changes and composition, particle size and morphology of the resulted $La_{0.6}Sr_{0.4}M_{0.1}Fe_{0.9}O_{3-\delta}$ (M: Co, Ni and Cu) nanostructures prepared by sonochemical synthesis and compare their mechanical characterizations. In this regard, I would be thankful to you if you could kindly consider our manuscript and do the needful for favor publication.

This manuscript describes our original research investigation and not submitted elsewhere for publication.

Thanking You,

Yours sincerely,

ALI AKBARI-FAKHRABADI
Assistant Professor
Department of Mechanical Engineering
Faculty of Mathematical and Physical Sciences
University of Chile, Santiago, CHILE
Phone: +56 229784690
E-mail: aliakbarif@ing.uchile.cl

Structural and mechanical properties of $La_{0.6}Sr_{0.4}M_{0.1}Fe_{0.9}O_{3-\delta}$ (M: Co, Ni and Cu) perovskites

A. Akbari-Fakhrabadi*[,a], V. Meruane[a], M. Jamshidijam[b], M.A. Gracia-Pinilla [c,d], R. Garcia[e], M. Orellana[a]

[a]Advanced Materials Laboratory, Department of Mechanical Engineering, University of Chile, Santiago, Chile

[b] Department of Materials Engineering, Islamic Azad University, Sirjan Branch, Sirjan, Iran

[c]Universidad Autónoma de Nuevo León, Facultad de Ciencias Físico-Matemáticas, Av. Universidad, Cd. Universitaria, San Nicolás de los Garza, N.L., Mexico

[d]Universidad Autónoma de Nuevo León, Centro de Investigación e Innovación en Desarrollo de Ingeniería y Tecnología, PIITKm6, Carretera al Aeropuerto, Apodaca, N.L., Mexico

[e]Universidad de Concepcion, Facultad de Ciencias Qu´ımicas, Edmundo Larenas 129, Concepcion, Chile

E-mail: aliakbarif@ing.uchile.cl

Abstract

$La_{0.6}Sr_{0.4}M_{0.1}Fe_{0.9}O_{3-\delta}$ (M: Co, Ni and Cu) perovskite nanostructures were synthesized using low frequency ultrasound assisted synthesis technique and effect of substitution of Fe by Co, Ni and Cu on crystal structure and mechanical properties in $La_{0.6}Sr_{0.4}FeO_{3-\delta}$ perovskite were studied. The HRTEM and Rietveld refinement analyses revealed the uniform equi-axial shape of the obtained nanostructures with the existence of $La_{0.6}Sr_{0.4}M_{0.1}Fe_{0.9}O_{3-\delta}$ with mixed rhombohedral and orthorhombic structures. Substitution of Cu decreases the melting point of $La_{0.6}Sr_{0.4}FeO_{3-\delta}$. The results of mechanical characterizations show that $La_{0.6}Sr_{0.4}Co_{0.1}Fe_{0.9}O_{3-\delta}$ and $La_{0.6}Sr_{0.4}Ni_{0.1}Fe_{0.9}O_{3-\delta}$ have ferroelastic behavior and comparable elastic moduli, however, subtitution of Ni shows higher hardness and lower fracture toughness than Co in B-site doping.

Keywords: Perovskite; ultrasound assisted synthesis; structure; mechanical properties.

Introduction

Reversible solid oxide cell (RSOC) technology as a solid-state and high efficient electrochemical energy conversion device is one of the most promising electricity storage/generation options and has been projected as a key component of the future electric grid to increase efficiency and allows large-scale penetration of intermittent renewable resources [1-3]. It is constructed of a membrane electrode assembly comprising a laminated fuel electrode, solid electrolyte and oxygen electrode. Due to high temperature operation and having highly exothermic and endothermic reactions during fuel and electrolysis cell modes, respectively, one significant challenge of designing RSOC system is its thermal management and long term stability and durability [4, 5].

The developments of perovskite materials with a flexible crystal structure (ABO_3) have received many attentions as their structures can be tailored by doping and/or co-doping strategies and obtain various properties accordingly. It has been demonstrated that the appropriate selection of the A- and B-site elements (or element combinations) can change their electrical and electrochemical characteristics and thus render them more useful as SOFC components materials [6, 7]. Lanthanum-based perovskite-structured material with general formula of $La_{1-x}Sr_xCo_yFe_{1-y}O_{3-d}$ (LSCF) has been extensively studied due to its promising mixed electronic–ionic conductivity and high oxygen surface exchange rate as an oxygen electrode material [8]. However, the formation of insulating secondary phases and cations inter-diffusion across the interface of electrolyte/electrode layers have been observed due to the high diffusivity of the metal component such as Co [9] in perovskite structure which has a large flexibility and can accept a variety of cations. To suppressing this drawback, the feasibility of other transition metals substitution in the B-site in LSCF

was investigated and cobalt-free perovskite structures such as $La_{0.6}Sr_{0.4}Fe_{0.8}Cu_{0.2}O_{3-d}$ [10] and $La_{0.6}Sr_{0.4}Fe_{0.9}Ni_{0.1}O_{3-d}$ [11] have been developed.

Despite many studies have concentrated on conduction properties and performance of newly developed perovskite materials, their associated mechanical properties studies is limited in the literature. In this investigation, $La_{0.6}Sr_{0.4}Fe_{0.9}M_{0.1}O_{3-d}$ (M: Co, Ni and Cu) was prepared by low frequency ultra sound assisted synthesis method to study and compare their structural and mechanical characterizations.

Experimental

The stoichiometric proportions of La, Sr, M (Co, Ni and Cu) and Fe nitrate precursors were dissolved in distilled water by magnetic stirring in order to obtain a homogeneous solution. NaOH solution was added to the precursor solution under vigorous mechanical stirring along with the ultrasonic irradiation (~50 kHz) for an hour. The role of NaOH was to maintain the pH during the synthesis of $La_{0.6}Sr_{0.4}M_{0.1}Fe_{0.9}O_{3-\delta}$ nanomaterials. The subsequent filtration of the obtained material was performed. The filtered residues were re-dispersed and washed with distilled water for several times until the washed solution reaches neutral pH. Finally, the obtained materials were dried and then calcined at 800 ºC for 2 hours. The details of the synthesis have been reported elsewhere [12]. The thermal analysis of the as-dried materials was characterized by thermo-gravimetric (TG) analysis using Netzsch-STA 449C.

The calcined nanopowders were characterized by X-ray diffraction (XRD, Bruker D8) using TOPAS software and transmission electron microscopy (Tecnai F20 FEG and FEI TITAN G2 80-300) analyses to study for their structure, particle size and chemical analysis.

The calcined powders were uni-axially pressed (90 MPa) to fabricate discs (D=25 and t=3 mm) and bars (3×5×30 mm) which were sintered at 1250°C for 2h. The structural characteristics of sintered discs were analysed by XRD with the same equipment and steps size of 0.001º. The discs were suspended by soft springs to simulate a "free-free" boundary condition and were excited by an impact hammer. The vibration of the discs is captured by a microphone which was connected to a data acquisition system. Once the experimental resonant frequencies were identified, the elastic modulus was computed using the following relationship [13]:

$$f_{20} = \frac{0.2458h}{r^2}\sqrt{\frac{E}{\rho(1-\nu^2)}}, \quad f_{01} = 1.682 f_{20} \tag{1}$$

where υ=0.3 is poisson´s ratio, h and r are thickness and radius of disc, respectively. The variables f_{20} and f_{01} correspond to the first two resonant frequencies of the disc. The details of the method have been reported elsewhere [14]. Bars were used in three-point bending tests using Zwick/Roell Z2.5 TN testing machine with a crosshead speed of 0.5 mm/min and a span width of 20 mm at room temperature.

The Vickers microhardness of the sintered discs was measured using Struers microhardness tester under ambient conditions. The hardness was determined by the ratio of the applied load via a geometrically defined indenter to the projected area of the resultant impression using relationship:

$$H_v = \frac{1854.4P}{a^2} \tag{2}$$

where *P* is the applied load and *a* is the indentation diagonal length. In a typical indentation test, load was varied from 5 to 20N for a dwelling time of 15s. At least ten indentations were made for each load on all the samples. The fracture toughness was calculated by the

indentation technique using the same instrument. Both diagonal lengths of the indentation images and crack lengths were measured by scanning electron microscopy (SEM) and the fracture toughness (K_{IC}) values were calculated by the method of Palmqvist cracks.

Results and discussion

Fig. 1 shows the thermal characteristics of the as-dried nanomaterials, which demonstrate the reactant precursors undergoes similar two stages of decomposition followed by the crystallization phases which resulted in the range of 16 to 22% of total weight loss until 900°C. An initial weight loss was noticed up to 400°C that corresponds to the evaporation of surface water and the dehydration of the nanomaterial. The second weight losses were perceived between 400 and 800°C attributed to the decomposition of carbonates such as lanthanum carbonate which explained elsewhere [12].

The XRD patterns of calcined powders and sintered discs were indexed and analyzed by Rietveld refinement using the perovskite models of $La_{0.6}Sr_{0.4}FeO_3$ (LSF) with space group of R-3c (rhombohedral) and Pnma (orthorhombic) with fixed site occupancy factors to the nominal values and pseudo Voigt peak shape. The temperature factors of the La/Sr and Fe/M (M: Co, Ni and Cu) sites were constrained to be the same values reported by Sora et al. [15]. As shown in Fig. 2 and Table 1-3, all three calcined nanopowders were mixtures of rhombohedral and orthorhombic phases with MFe_2O_4 (M: Co, Ni and Cu) as secondary phases. Additionally, La_2CuO_4 were detected in $La_{0.6}Sr_{0.4}Cu_{0.1}Fe_{0.9}O_{3-d}$. Fig. 3 and Table 4-6 demonstrate XRD patterns and structure parameters and factors of Reitveld refinement of sintered discs, which show that the weight percent of orthorhombic phase in all three materials has been increased and La_2CuO_4 decomposed in $La_{0.6}Sr_{0.4}Cu_{0.1}Fe_{0.9}O_{3-d}$ after

sintering. MFe_2O_4 formation is in contrary to Zhang [11] and Vogt et al. [16] reports in which it is claimed that Ni and Cu substitutions upto 20 mol% leads to single-phase perovskites. Carnna et al. [17] also reported a small amount of La_2CuO_4 in $LaFe_{0.6}Cu_{0.4}O_3$ prepared by citrate auto-combustion synthesis method and claimed lanthanum ferrites free from impurities in copper molar content of lower than 0.4.

The HRTEM micrographs and SAED pattern of the $La_{0.6}Sr_{0.4}Ni_{0.1}Fe_{0.9}O_{3-\delta}$, $La_{0.6}Sr_{0.4}Co_{0.1}Fe_{0.9}O_{3-\delta}$ and $La_{0.6}Sr_{0.4}Cu_{0.1}Fe_{0.9}O_{3-\delta}$ calcined nanopowders are presented in Fig. 4. As it can be seen from the micrographs, they consist of nano-sized equi-axial shape particles with high crystallinity and an average particle size less than 50 nm. As it can be seen in Fig. 4b, d and f, all samples showed the (110) lattice fringes encountered for LSF (2.80 Å) and the (3.90Å) lattice fringes that correspond to (012) of LSCuF were demonstrated.

LSCuF samples sintered at 1250 ºC/2h were deformed due to lower melting point of these samples containing copper in B-site of perovskite structure, which were also reported by Vogt et al. [16]. Therefore, further characterizations were done on LSCF and LSNF perovskites. Table 7 shows the elastic properties of prepared LSCF and LSNF perovskites calculated by impulse excitation technique as high precision dynamic method [18]. The frequencies obtained by this method were used along with bulk densities measured by geometrical method in equation 1 to calculate Young's modulus which is a function of temperature, porosity, chemical composition and oxygen vacancy concentration and can be expressed as

$$E = E_0 \exp(-4.5P) \tag{3}$$

where E_0 is the elastic modulus at zero porosity (P=0) [19]. The porosity of sintered discs were obtained by comparing bulk density and theoretical density of discs which calculated using crystallographic density of each phase and its corresponding weight percent obtained by XRD analyses by the rule of mixture. As it can be seen in Table 2, E_0 of the samples were calculated to avoid the effect of porosity, which shows that LSCF and LSNF have comparable elastic modulus.

As a property that indirectly reveals the bulk mechanical strength of the sintered ceramics, microhardness of LSCF and LSNF prepared discs were measured and compared. As shown in Fig. 5, LSNF showed higher microhardness than that of LSCF and $La_{0.6}Sr_{0.4}Co_{0.2}Fe_{0.8}O_{3-d}$ reported by Chou et al. [20] and comparable microhardness with that of $La_{0.58}Sr_{0.4}Co_{0.2}Fe_{0.8}O_{3-d}$ [21]. The cracks observed near the indentation zones were used to calculate the indentation fracture toughness. There are many equations with some conditions and limitations proposed for measuring indentation fracture toughness. For comparison purpose, fracture toughness was determined by Niihara's [22], Laugier's [23], Anstis's [24] and Evan's [25] equations. As graphed in Fig. 6, LSCF showed higher fracture toughness. Both materials show higher fracture toughness than that of $La_{0.6}Sr_{0.4}Co_{0.2}Fe_{0.8}O_{3-d}$ [20] and $La_{0.58}Sr_{0.4}Co_{0.2}Fe_{0.8}O_{3-d}$ [21, 26].

As structural changes due to ferroelastic to paraelastic transition have been reported in LSCF perovskite [26, 27], prepared LSCF and LSNF perovskites were studied by typical load–displacement curves measured by three-point bending tests at room temperature as shown in Fig. 7. As it can be seen, both LSCF and LSNF perovskites demonstrate a non-linear deformation at lower loads due to rhombohedral symmetry which allows formation of domains induced my mechanical stresses upto a deviation point onwards switching to linear deformation until fracture [27].

4. Conclusions

Effect of B-site cation doping with Co, Ni and Cu on stracutal and mechanical propoerties of $La_{0.6}Sr_{0.4}FeO_{3-\delta}$ perovskite synthesizd by low frequency ultrasound assisted method was investigated. The nanocrystalline $La_{0.6}Sr_{0.4}M_{0.1}Fe_{0.9}O_{3-\delta}$ (M: Co, Ni and Cu) perovskites with mixed rhombohedral and orthorhombic structures having MFe_2O_4 secondary phases in all calcined nanopowders and sintered discs were obtained. Doping Fe by Cu also showed La_2CuO_4 phase in calcined nanopowders, which decomposed by sintering and lowered the melting point. The results of mechanical characterizations show that LSCF and LSNF have ferroelastic behavior and comparable elastic moduli, however, LSNF show higher hardness and lower fracture toughness.

Acknowledgements

The first author acknowledges FONDECYT, Government of Chile (Projects No.: 3140180 and 11160202), for the support to carry out this project.

References

1. D. Ferrero, A. Lanzini, P. Leone, M. Santarelli, Chem. Eng. J. 274 (2015) 143–55.
2. V.N. Nguyen, L. Blum, Compendium of Hydrogen Energy 3 (2016) 115-45.
3. Y.S. Yoo, M. Choi, J.H. Hwang, H.N. Im, B. Singh, S. J. Song, Ceram. Int. 41 (2015) 6448–54.
4. C.H. Wendel, P. Kazempoor, R.J. Braun, J. Power Sources 276 (2015) 133-44.
5. L. Barelli, G. Bidini, G. Cinti, A. Ottaviano, Energy Convers. Manage. 117 (2016) 289–96.
6. J. Richter, P. Holtappels, T. Graule, T. Nakamura, L.J. Gauckler, Monatsh. Chem. 140 (2009) 985–99.

7. A. Ecija, K. Vidal, A. Larrañaga, A. Martínez-Amesti, L. Ortega-San-Martín, M.I. Arriortua, Solid State Ionics 201 (2011) 35–41.

8. Z. Chen, X. Wang, V. bhakhri F. Giuliani, A. Atkinson, Acta Mater. 61 (2013) 5720–34.

9. N. Sakai, T. Horita, K. Yamaji, M.E. Brito, et al., J. Electrochem. Soc 153 (2006) A621-25.

10. Q. Zhou, L. Xu, Y. Guo, D. Ja, et al., Int. J. Hydrogen Energy 37 (2012) 11963-68.

11. F. Zhang, Z. Yang, H. Wang, W. Wang, G. Ma, FUEL CELLS 12 (2012) 749–53.

12. A. Akbari-Fakhrabadi, P. Sathishkumar, K. Ramam, R. Palma, R.V. Mangalaraja, Powder Technology, 276, 2015, 200-203.

13. L. Meirovitch Analytical methods in vibration. New York, NY.: The Mcmillan Company 19 (1967).

14. A. Akbari-Fakhrabadi, V. Meruane, M. Jamshidijam, R. V. Mangalaraja, Miguel A. Gracia, Materials Science and Engineering A, 649, 2016, 168-173.

15. I.N. Sora, T. Caronna, F. Fontana, C.J. Fernandez, et al., J. Solid state Chemistry 191 (2012) 33-39.

16. U.F. Vogt, P. Holtappels, J. Sfeir, J. Richter, , et al., Fuel cells, 09 (2009) 899-906.

17. T. Caronna, F. Fontana, I.N. Sora, R. Pelosato, Materials Chemistry and Physics 116 (2009) 645–648.

18. M. Radovic, E. Lara-Curzio, L. Riester, Mater. Sci. Eng. A368 (2004) 56–70.

19. X.F. Fan, E.D. Casen, Q. Yang, J.D. Nicholas, Ceram. Int. 39 (2013) 6877–86.

20. Y.S. Chou, J.W. Stevenson, T.R. Armstrong, L. Pederson, J. Am. Ceram. Soc. 83 (2000) 1457–64.

21. N. Li, A. Verma, P. Singh, J.H. Kim, Ceramics International 39 (2013) 529–538.

22. K. Niihara, R. Morena, D.P.H. Hasselman, J. Mater. Sci. Lett. 2 (1983) 221-223.

23. M.T. Laugier, J. Mater. Sci. Lett. 4 (1985) 1539–1541.

24. G.R. Anstis, P. Chantikul, B.R. Lawn, D.B. Marshall, J. Am. Ceram. Soc. 64 (1981) 539-543.

25. A.G. Evans, E.A. Charles, J. Am. Ceram. Soc. 59 (1976) 371–372.

26. B.X. Huang, J. Malzbender, R.W. Steinbrech, E. Wessel, et al., J. of Membrane Science 349 (2010) 183–188.

27. B.X. Huang, R.W. Steinbrech, J. Malzbender, Solid State Ionics 228 (2012) 32–36.

Tables and figures Captions

Table 1. The structure parameters and XRD refinement results of LSCF nanopowders calcined at 800 ºC/2h.

Table 2. The structure parameters and XRD refinement results of LSNF nanopowders calcined at 800 ºC/2h.

Table 3. The structure parameters and XRD refinement results of LSCuF nanopowders calcined at 800 ºC/2h.

Table 4. The structure parameters and XRD refinement results of LSCF discs sintered at 1250 ºC/2h.

Table 5. The structure parameters and XRD refinement results of LSNF discs sintered at 1250 ºC/2h.

Table 6. The structure parameters and XRD refinement results of LSCuF discs sintered at 1250 ºC/2h.

Table 7. Physical and elastic properties of LSCF and LSNF discs sintered at1250 °C/2h.

Fig. 1. Thermogravimetric analysis curves of as dried nanomaterials.

Fig. 2. XRD patterns of LSCF, LSNF and LSCuF nanopowders calcined at 800 °C for 2 h.

Fig. 3. XRD patterns of LSCF, LSNF and LSCuF discs sintered at 1250 °C for 2 h.

Fig. 4. HRTEM micrographs and SAED patterns of (a, b) LSCF, (c, d) LSNF and (e, f) LSCuF nanopowders calcined at 800 ºC for 2 h.

Fig. 5. Microhardness of LSCF and LSNF sintered discs as a function of load.

Fig. 6. Fracture toughness measured with Niihara,Laugier,Anistis and Evan's Eqs. at 10 N applied load for LSCF and LSNF sintered discs.

Fig. 7. Typical load-displacement curves of LSCF and LSNF during three-point bending at room temperature.

Table 1.

Space group	Pnma	R-3c
a (Å)	5.5258	5.5302
b (Å)	7.8449	
c (Å)	5.5359	13.5744
ρ (gcm^{-3})	6.159	7.497
Crystal size (nm)	60	47
La/Sr x/a, y/b, z/c	-0.02495, 0.25, 1.0004	0.00, 0.00, 0.25
Fe/Co x/a, y/b, z/c	0.00, 0.00, 0.5	0.00, 0.00, 0.00
O(1) x/a, y/b, z/c	0.5, 0.25, 0.1594	0.5299, 0.05992, 0.25
O(2) x/a, y/b, z/c	0.559, 0.03879, 0.67489	
R (Bragg)	0.443	0.418
Wt%	39	60
Impurities (Wt%)	$CoFe_2O_4$ (~1)	
R_{exp} (%)	3.11	
R_{wp} (%)	3.47	
R_p (%)	2.72	
GOF	1.12	

Table 2.

Space group	Pnma	R-3c
a (Å)	5.5450	5.5474
b (Å)	7.8401	
c (Å)	5.5423	13.5898
ρ (gcm^{-3})	6.134	7.442
Crystal size (nm)	61	38
La/Sr x/a, y/b, z/c	-0.02181, 0.25, 0.99797	0.00, 0.00, 0.25
Fe/Ni x/a, y/b, z/c	0.00, 0.00, 0.5	0.00, 0.00, 0.00
O(1) x/a, y/b, z/c	0.5, 0.25, -0.0688	0.49355, -0.08571, 0.25
O(2) x/a, y/b, z/c	0.6462, 0.2196, 0.76515	
R (Bragg)	0.363	0.173
Wt%	50	47
Impurities (Wt%)	$NiFe_2O_4$ (~3)	
R_{exp} (%)	2.00	
R_{wp} (%)	2.36	
R_p (%)	1.86	
GOF	1.18	

Table 3.

Space group	Pnma	R-3c
a (Å)	5.5499	5.5556
b (Å)	7.8377	
c (Å)	5.5521	13.5316
ρ (gcm^{-3})	6.133	7.465
Crystal size (nm)	80	99
La/Sr x/a, y/b, z/c	-0.02552, 0.25, 0.99746	0.00, 0.00, 0.25
Fe/Cu x/a, y/b, z/c	0.00, 0.00, 0.5	0.00, 0.00, 0.00
O(1) x/a, y/b, z/c	0.5, 0.25, 0.4999	0.43661, -0.00681, 0.25
O(2) x/a, y/b, z/c	0.76332, 0.04676, 0.75048	
R (Bragg)	2.114	0.568
Wt%	44	43
Impurities (Wt%)	La_2CuO_4 (~12), $CuFe_2O_4$ (~2)	
R_{exp} (%)	2.05	
R_{wp} (%)	2.70	
R_p (%)	2.06	
GOF	1.32	

Table 4.

Space group	Pnma	R-3c
a (Å)	5.5015	5.5389
b (Å)	7.7873	
c (Å)	5.5461	13.4978
ρ (gcm^{-3})	6.221	7.516
Crystal size (nm)	66	73
La/Sr x/a, y/b, z/c	0.02003, 0.25, 0.99952	0.00, 0.00, 0.25
Fe/Co x/a, y/b, z/c	0.00, 0.00, 0.5	0.00, 0.00, 0.00
O(1) x/a, y/b, z/c	0.5, 0.25, 0.48948	0.59204, 0.07834, 0.25
O(2) x/a, y/b, z/c	0.50567, 0.05323, 0.57699	
R (Bragg)	0.985	0.87
Wt%	38	60
Impurities (Wt%)	$CoFe_2O_4$ (~2)	
R_{exp} (%)	1.07	
R_{wp} (%)	2.58	
R_p (%)	1.77	
GOF	2.40	

Table 5.

Space group	Pnma	R-3c
a (Å)	5.5304	5.5881
b (Å)	7.8263	
c (Å)	5.5508	13.5822
ρ (gcm^{-3})	6.152	7.338
Crystal size (nm)	105	59
La/Sr x/a, y/b, z/c	0.02386, 0.25, 1.00556	0.00, 0.00, 0.25
Fe/Ni x/a, y/b, z/c	0.00, 0.00, 0.5	0.00, 0.00, 0.00
O(1) x/a, y/b, z/c	0.5, 0.25, 0.48945	0.50094, 0.12401, 0.25
O(2) x/a, y/b, z/c	0.75238, 0.01142, 0.75215	
R (Bragg)	2.627	1.112
Wt%	54	42
Impurities (Wt%)	$NiFe_2O_4$ (~4)	
R_{exp} (%)	1.11	
R_{wp} (%)	2.68	
R_p (%)	1.81	
GOF	2.42	

Table 6.

Space group	Pnma	R-3c
a (Å)	5.5447	5.5852
b (Å)	7.8359	
c (Å)	5.5576	13.6027
ρ (gcm^{-3})	6.134	7.347
Crystal size (nm)	126	168
La/Sr x/a, y/b, z/c	0.02307, 0.25, 0.99727	0.00, 0.00, 0.25
Fe/Cu x/a, y/b, z/c	0.00, 0.00, 0.5	0.00, 0.00, 0.00
O(1) x/a, y/b, z/c	0.5, 0.25, 0.19956	0.49387, 0.10636, 0.25
O(2) x/a, y/b, z/c	0.76124, 0.01925, 0.75683	
R (Bragg)	2.268	0.773
Wt%	78	20
Impurities (Wt%)	$CuFe_2O_4$ (~2)	
R_{exp} (%)	1.70	
R_{wp} (%)	2.53	
R_p (%)	1.93	
GOF	1.49	

Table 7.

	$f_{20} \times 10^4$ (Hz)	$f_{01} \times 10^4$ (Hz)	Measured density (gcm^{-3})	Relative density (%)	E (GPa)	E_0 (GPa)
LSCF	2.839	4.79	5.69	84.5	134.6	269.9
LSNF	2.910	4.77	5.82	87.2	153.9	274.0

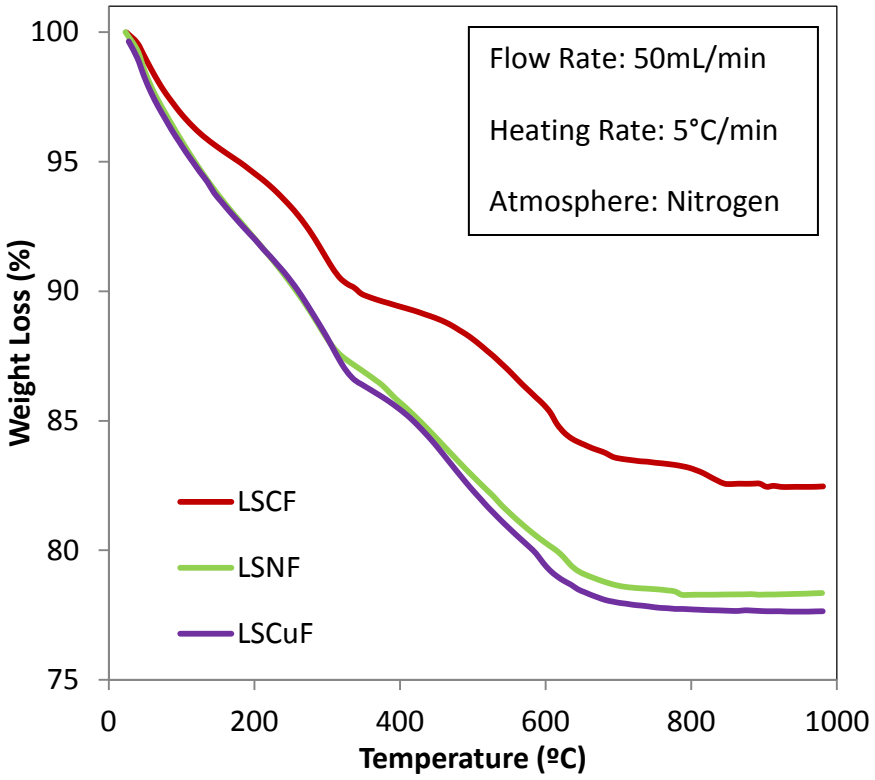

Fig. 1.

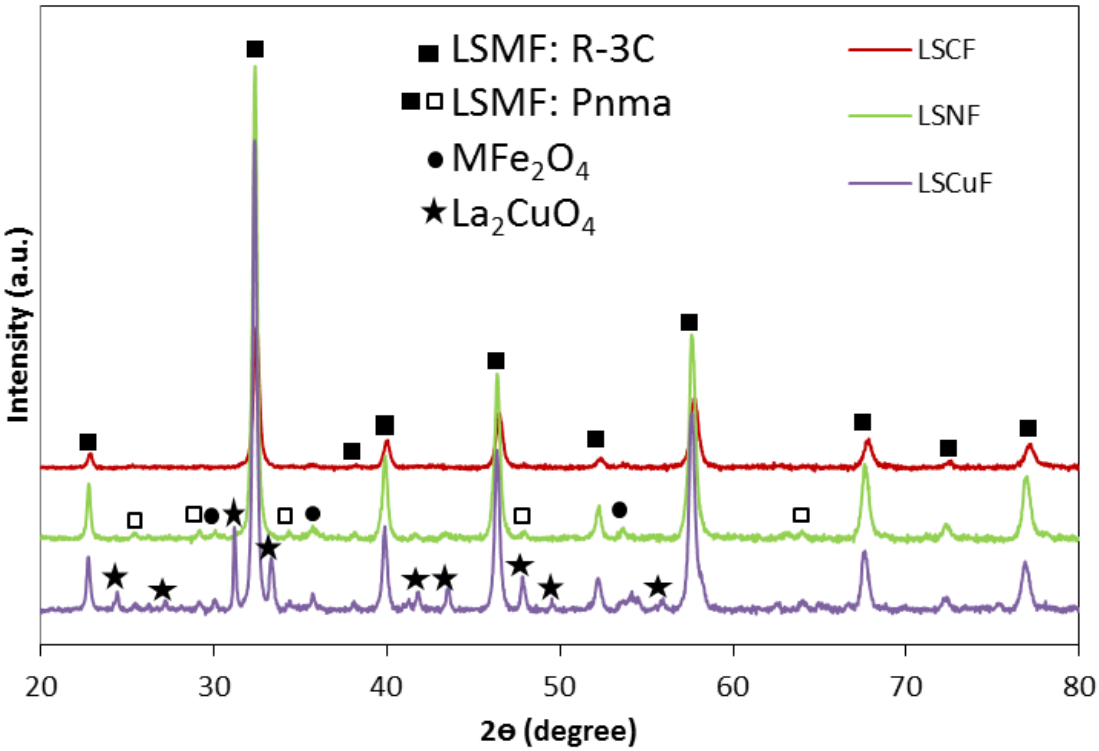
LSMF: R-3C
LSMF: Pnma
MFe2O4
La2CuO4
LSCF
LSNF
LSCuF
Intensity (a.u.)
20
30
40
50
60
70
80
2θ (degree)

Fig. 2.

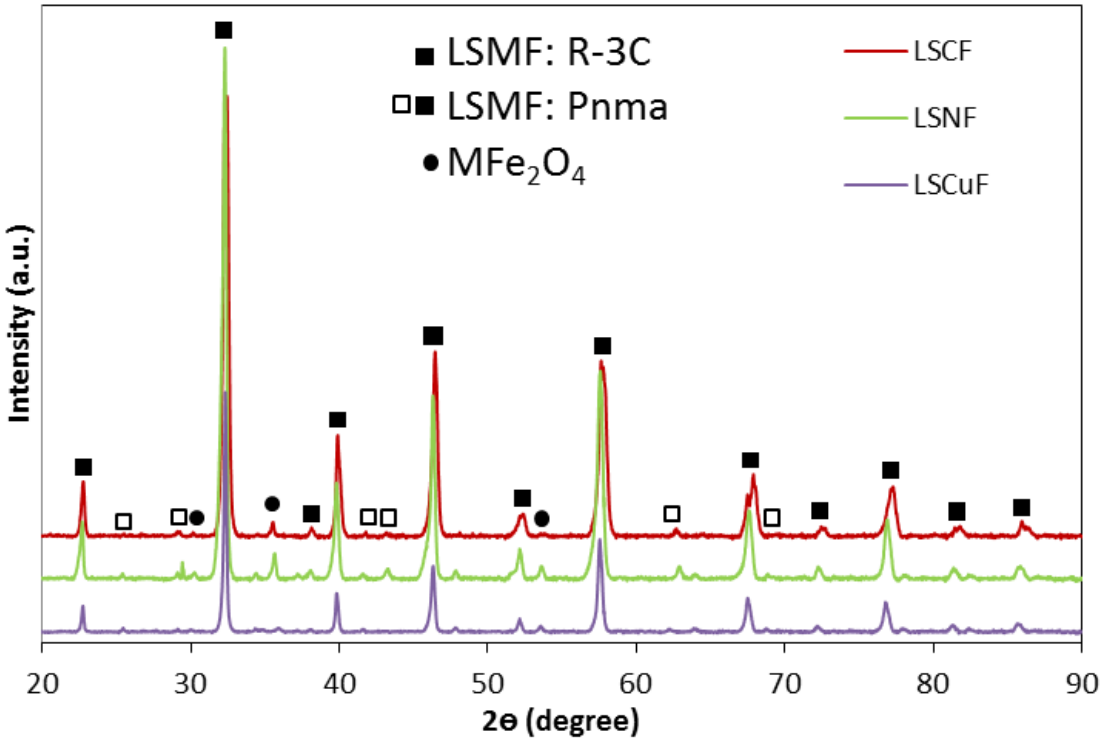
LSMF: R-3C
LSMF: Pnma
MFe2O4
LSCF
LSNF
LSCuF
Intensity (a.u.)
20
30
40
50
60
70
80
90
2θ (degree)

Fig. 3.

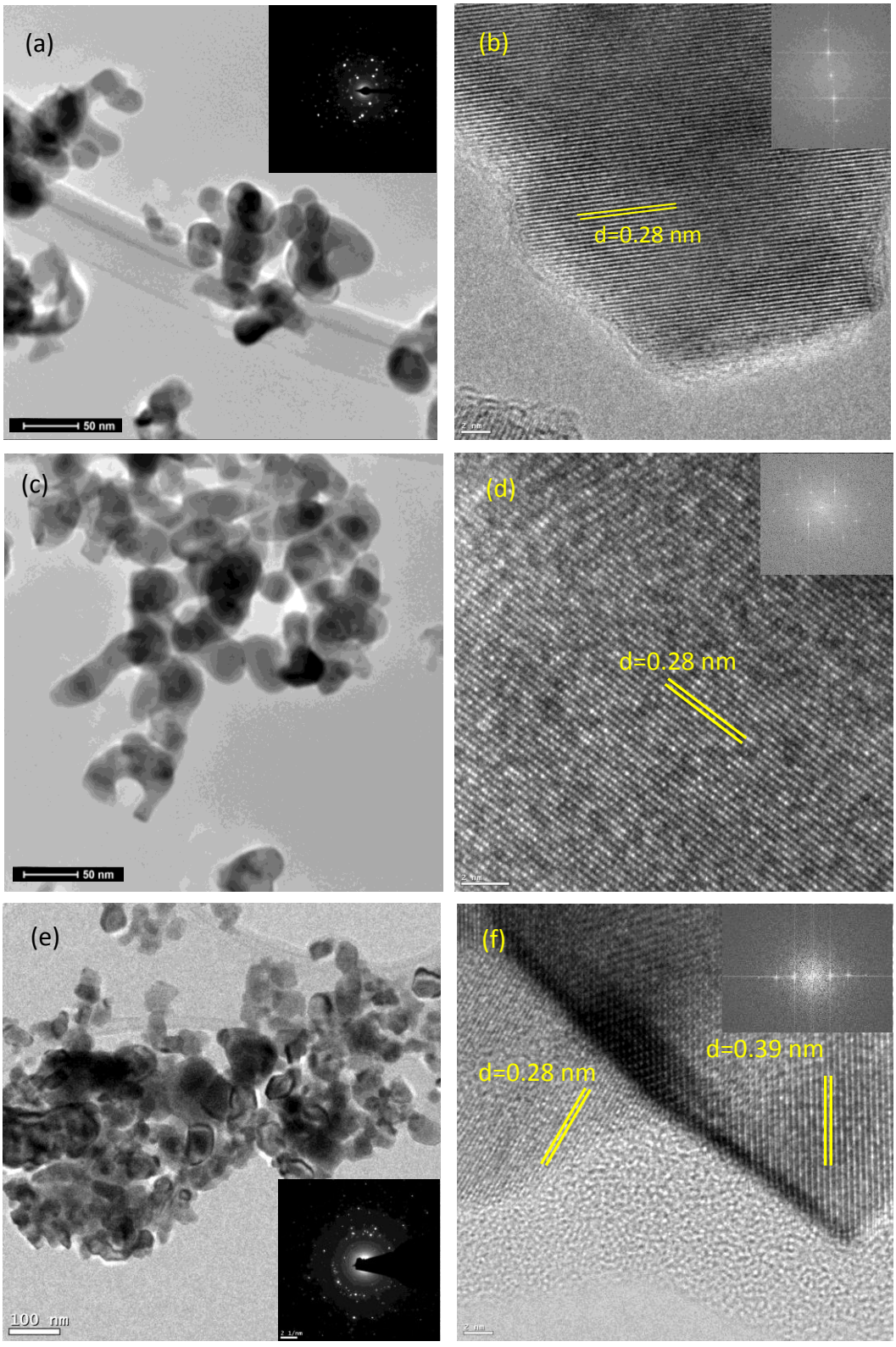

Fig. 4.

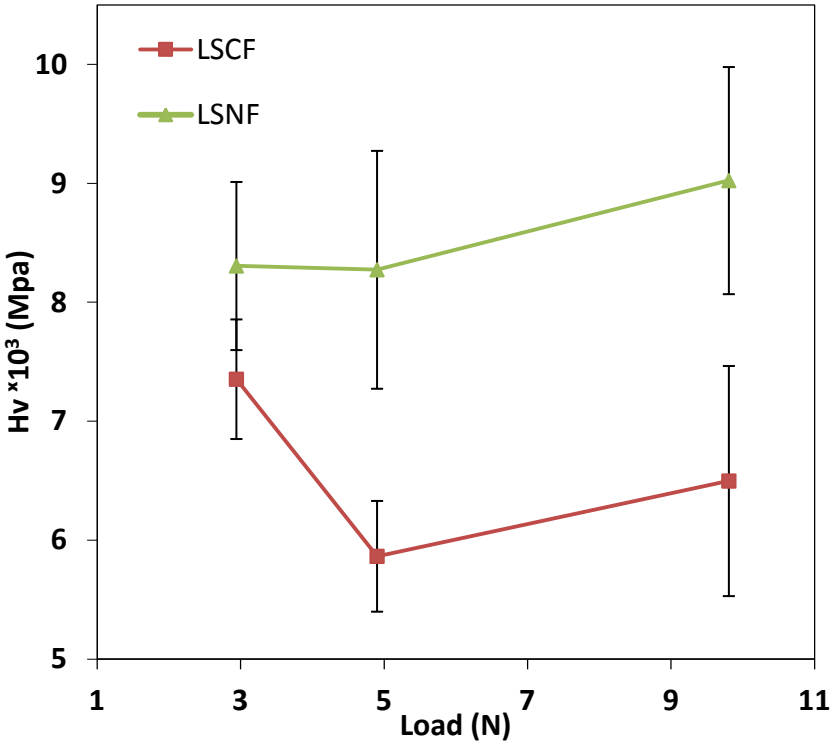
LSCF
LSNF
10
9
8
7
6
5
Hv ×10³ (Mpa)
1
3
5
7
9
11
Load (N)

Fig.5.

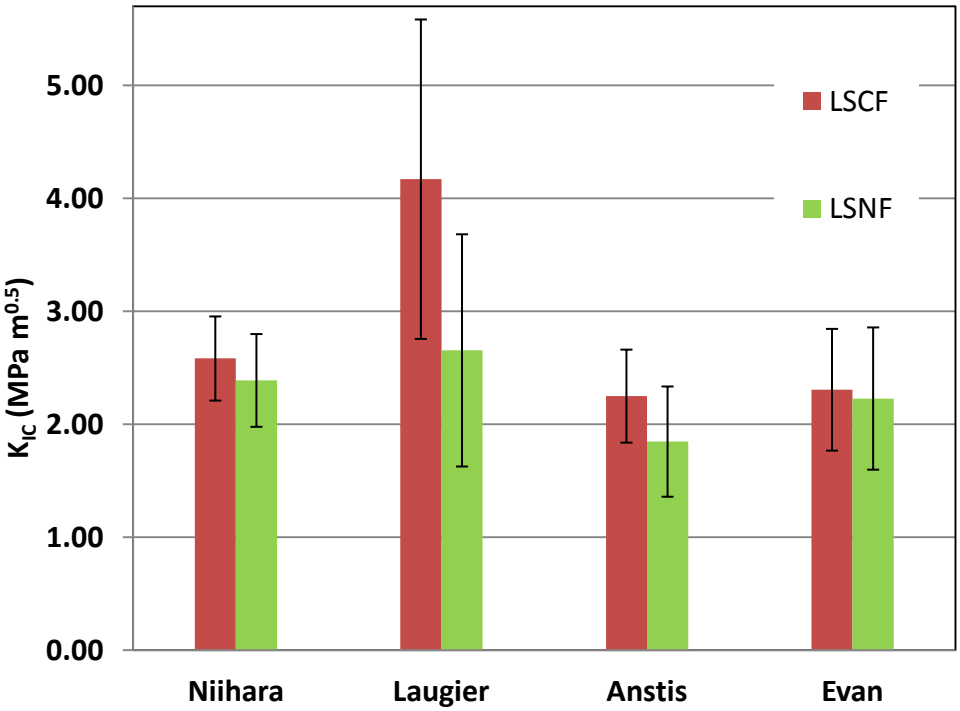
LSCF
LSNF
5.00
4.00
3.00
2.00
1.00
0.00
K_IC (MPa m^0.5)
Niihara
Laugier
Anstis
Evan

Fig. 6.

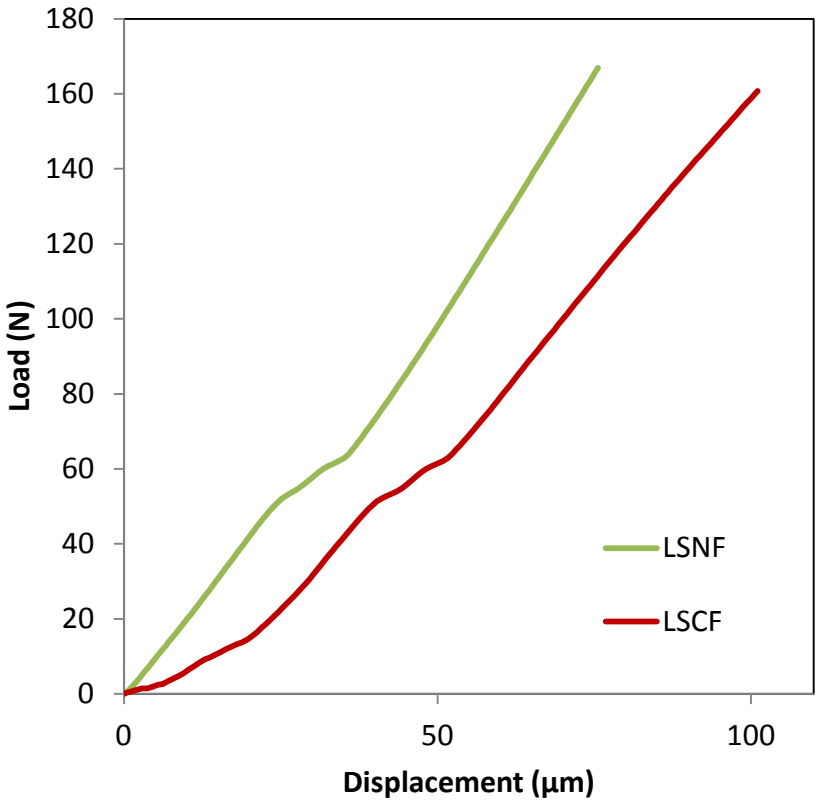
180
160
140
120
100
80
60
40
20
0
Load (N)
0
50
100
Displacement (µm)
LSNF
LSCF

Fig. 7.

e-component

Click here to download e-component: supplementary.docx